arXiv:1511.06158v1 [nucl-th] 19 Nov 2015

Shape coexistence in the microscopically guided interacting boson model

K. Nomura[1]‡, **T. Otsuka**[2,3,4], **and P. Van Isacker**[1]

[1] Grand Accélérateur National d'Ions Lourds, CEA/DSM-CNRS/IN2P3, B. P. 55027, F-14076 Caen Cedex 5, France
[2] Department of Physics, University of Tokyo, Hongo, Bunkyo-ku, Tokyo 113-0033, Japan
[3] Center for Nuclear Study, University of Tokyo, Hongo, Bunkyo-ku, Tokyo 113-0033, Japan
[4] National Superconducting Cyclotron Laboratory, Michigan State University, East Lansing, Michigan 48824, USA

E-mail: nomura@ikp.uni-koeln.de

November 2015

Abstract. Shape coexistence has been a subject of great interest in nuclear physics for many decades. In the context of the nuclear shell model, intruder excitations may give rise to remarkably low-lying excited 0^+ states associated with different intrinsic shapes. In heavy open-shell nuclei, the dimension of the shell-model configuration space that includes such intruder excitations becomes exceedingly large, thus requiring a drastic truncation scheme. Such a framework has been provided by the interacting boson model (IBM). In this article we address the phenomenon of shape coexistence and its relevant spectroscopy from the point of view of the IBM. A special focus is placed on the method developed recently which makes use of the link between the IBM and the self-consistent mean-field approach based on the nuclear energy density functional. The method is extended to deal with various intruder configurations associated with different equilibrium shapes. We assess the predictive power of the method and suggest possible improvements and extensions, by considering illustrative examples in the neutron-deficient Pb region, where shape coexistence has been experimentally studied.

Keywords: Shape coexistence, interacting boson model, energy density functional

1. Introduction

The study of shape coexistence and related collective excitations in atomic nuclei has been a theme of major interest in low-energy nuclear structure physics for more than half a century [1, 2, 3, 4, 5, 6]. In specific regions of the periodic table, unexpectedly low-lying excited 0^+ states close in energy to the 0^+ ground state have been observed. In the spherical shell model [3, 7, 8], the emergence of the low-lying excited 0^+ states has been often attributed to multi-particle-multi-hole intruder excitations. This scenario may hold in mass regions near shell closure, the example being the neutron-deficient lead region. In this case, two or four protons in the $Z = 50 - 82$ major

‡ Present address: Physics Department, Faculty of Science, University of Zagreb, HR-10000 Zagreb, Croatia

shell can be excited to the next major shell. The correlation between valence protons and neutrons is enhanced due to this cross-shell excitation of protons, resulting in the lowering of the excited 0^+ configurations. This effect becomes prominent especially around the middle of the neutron major shell $N = 104$, where the number of valence neutrons is maximal.

The shell-model approach [9, 10] has been a reliable means of studying spectroscopic properties relevant to shape coexistence in a quantitative way. However, the dimension of the configuration space becomes exceedingly large for open-shell heavy-mass nuclei, requiring a drastic truncation scheme to make the problem tractable. Such a framework has been provided by the interacting boson model (IBM) [11], in which the correlated pairs of valence nucleons, S ($J^\pi = 0^+$) and D (2^+), are mapped onto s and d bosons, respectively [12, 13, 14]. In the IBM, the number of proton (neutron) bosons, denoted by N_π (N_ν), is equal to that of pairs of valence protons (neutrons) [14]. The IBM is strongly connected to group theory: if the Hamiltonian is expressed as a specific combination of Casimir operators, the corresponding system has a dynamical symmetry associated with a certain intrinsic structure and is exactly solvable [11]. In the simplest version of the IBM consisting of only s and d bosons, for instance, three possible dynamical symmetries, U(5), SU(3) and SO(6), emerge, corresponding to vibrational, rotational and γ-unstable states of the quadrupole mode. The IBM has been well established for systematic and straightforward, albeit purely phenomenological, calculations of nuclear collective excitation energies and electromagnetic transition rates in medium- and heavy-mass nuclei.

A method to incorporate intruder excitations in the IBM was first presented by Duval and Barrett [15, 16]. They proposed to associate the different shell-model spaces of $0p-0h$, $2p-2h$, $4p-4h$, ... excitations with the corresponding boson spaces comprising N, $N+2$, $N+4$, ... bosons, with N being the total boson number $N = N_\pi + N_\nu$, and the different boson subspaces are subsequently mixed by a specific Hamiltonian (see Subsec. 2.1). The Duval-Barrett procedure has been applied to the study of spectroscopic properties mainly in the Pb region [17, 18, 19, 20, 21]. The concept of intruder analog states was introduced by means of a new quantum number, the I-spin or intruder spin [22, 23, 24], while geometrical features of configuration mixing IBM were addressed [25, 26, 27]. Similar to previous IBM calculations, the drawback of the configuration mixing IBM approach is that its Hamiltonian parameters are constrained only by known experimental data on intruder states.

Let us stress that many attempts have been made to establish a link between the IBM and more fundamental nuclear structure models [28, 29]. The prescription widely taken is the one developed by Otsuka et al. [14], often referred to as the Otsuka-Arima-Iachello (OAI) mapping, where a seniority-based shell-model state, expressed by low-spin S, D, ... pairs, is mapped onto the equivalent boson s, d, ... states. This method is, however, rather restricted to nuclei with near-spherical or γ-soft shapes [30], where the simple seniority classification is a reasonable approximation. The microscopic derivation of the IBM for nuclei with general shapes, particularly strongly deformed ones, has been under active investigation in the 1980s, but since then without much progress.

An entirely new method of deriving the IBM Hamiltonian was presented in Ref. [31], whose authors proposed to derive the IBM Hamiltonian by mapping the total energy surface, calculated within the self-consistent mean-field [e.g., Hartree-Fock-Bogoliubov (HFB)] approach using a microscopic nuclear energy density functional

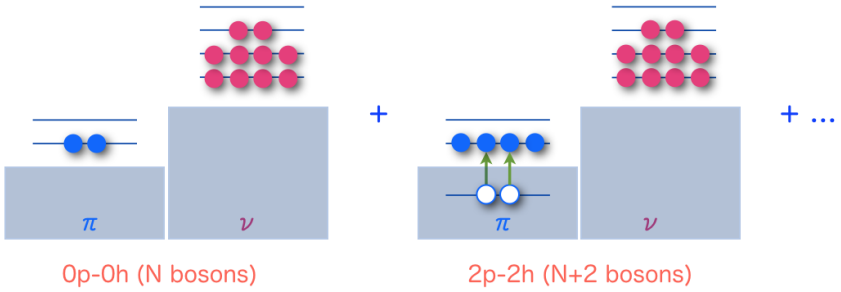

Figure 1. (Color online) Illustration of the configuration mixing in the IBM framework.

(EDF) onto the equivalent bosonic total energy surface. Self-consistent mean-field models on the basis of a given non-relativistic [32, 33, 34, 35] or relativistic [36, 37, 38] EDF are well established for the description of matter and bulk ground-state properties of almost all nuclei, including binding energies, charge radii *etc.* Their accuracy is remarkable and they can thus be suitable as microscopic input to the IBM for any deformed configuration. In this way, the IBM has been shown to be derived only from nucleonic degrees of freedom in principle for any deformed state, including near spherical or weakly deformed [39], strongly-deformed rotational [40], and γ-soft [41] regimes. Moreover, this allows one to have access to exotic isotopes [42]. Recently, the method of Ref. [31] was extended to handle shape coexistence [43] and applied to the neutron-deficient Pb [43] and Hg [44] nuclei and to some neutron-rich nuclei with mass $A \approx 100$ [45, 46].

We mention that calculations of nuclear spectroscopic properties have also been extensively pursued within beyond mean-field approaches [32, 47, 48, 49], by projecting the mean-field solution of an EDF calculation onto states with good symmetry and by taking into account quantum fluctuations around the mean-field minimum [32, 34].

This contribution gives a detailed description of the combined mean-field and IBM approach of Ref. [31], more in particular, its recent extension to the study of shape coexistence [43]. It also addresses the possibilities of the method for the future. The article is organized as follows: we give a brief overview of the relevant IBM framework in Sec. 2, describe the theoretical framework of the proposed method in Secs. 3 and 4 including some illustrative results for neutron-deficient Pb and Hg isotopes. Finally, Sec. 5 is devoted to concluding remarks and possible improvements and extensions of the method.

2. Interacting boson model for shape coexistence

2.1. Implementation of intruder configurations in the IBM

We first give a brief overview of the Duval-Barrett technique [15, 16] which allows one to mix different IBM configurations to describe low-lying excited intruder states. Throughout this article, we assume only proton excitations, because in all the cases considered here the proton number is close to the shell closure and cross-shell excitations of the protons can therefore be assumed more probable than those of neutrons.

In counting the number of bosons, Duval and Barrett followed the assumption that particle-like and hole-like bosons are not distinguished [15, 16]. Under this assumption, as the excitation of one proton pair (boson) increases the boson number by 2, the $np-nh$ ($n=0,2,4,\ldots$) configurations differ from each other in boson number by 2. Hence, to describe a system consisting of different intruder excitations, the boson Hilbert space is extended to the space $[N_\pi\otimes N_\nu]\oplus[(N_\pi+2)\otimes N_\nu]\oplus[(N_\pi+4)\otimes N_\nu]\oplus\cdots$, a direct sum of the orthogonal subspaces of the (N_π, N_ν), $(N_\pi+2, N_\nu)$, $(N_\pi+4, N_\nu)$, ... boson systems, respectively (see Fig. 1). In the following, the subspace $[(N_\pi+n)\otimes N_\nu]$ ($n=0,2,4,\ldots$) is denoted simply as $[N+n]$ with $N=N_\pi+N_\nu$.

Let us consider the ^{186}Pb nucleus as an example, as it is empirically known for the coexistence of three intrinsic shapes: spherical, oblate and prolate, corresponding to $0p-0h$, $2p-2h$ and $4p-4h$ shell-model configurations, respectively [5]. The total Hamiltonian is expressed as:

$$\hat{H}=\hat{P}_0\hat{H}_0\hat{P}_0+\hat{P}_2(\hat{H}_2+\Delta_2)\hat{P}_2+\hat{P}_4(\hat{H}_4+\Delta_4)\hat{P}_4+\hat{V}^{\rm mix}_{0,2}+\hat{V}^{\rm mix}_{2,4}, \quad (1)$$

where $\hat{H}_n$ ($n=0,2,4$) represent the unperturbed Hamiltonians for the proton $np-nh$ excitations in the shell model, and $\hat{V}^{\rm mix}_{n,n+2}$ ($n=0,2$) stand for the interaction terms mixing the $[N+n]$ and $[N+n+2]$ subspaces, defined as

$$\hat{V}^{\rm mix}_{n,n+2}=\hat{P}_{n+2}(\omega^s_{n,n+2}s^\dagger_\pi s^\dagger_\pi+\omega^d_{n,n+2}d^\dagger_\pi d^\dagger_\pi)^{(0)}\hat{P}_n+h.c., \quad (2)$$

where $\omega^s_{n,n+2}$ and $\omega^d_{n,n+2}$ represent the strengths of mixing. A direct coupling between $0p-0h$ and $4p-4h$ spaces is absent with two-body nuclear forces and is not considered here. The operators $\hat{P}_n$ ($n=0,2,4$) are projectors onto the subspace $[N+n]$, and Δ_{n+2} ($n=0,2$) represent the energies needed to excite one or two proton pair (or boson) across the shell closure $Z=82$. The parameters for each unperturbed Hamiltonian are fitted to the corresponding intruder bands. The values of the Hamiltonian parameters can be different from one configuration to another. The off-set energies Δ_{n+2} are usually determined to reproduce the bandhead 0^+ energies of intruder bands. The mixing strengths are often introduced perturbatively with small values relative to the Hamiltonian parameters.

Initially, the Duval-Barrett procedure was applied to Hg isotopes in Refs. [15, 16], followed by Refs. [50, 51] for the description of new data. It was also applied to different mass regions, including the Mo [16, 52] and Cd [53] isotopes. An application to Ge isotopes was presented [54] with separate treatment of particle-like and hole-like bosons in the mixing interaction. More recently, both spectroscopic and ground-state properties of nuclei showing manifest shape coexistence were extensively studied for the chains of Pb [17, 18, 19], Hg [20] and Pt [21] isotopes. On the other hand, the evidence for coexistence is somewhat hindered in Pt isotopes, and whether or not the intruder configuration is necessary in the IBM framework for Pt isotopes is still a matter of controversy [21, 55, 56, 57, 58].

2.2. Microscopy of configuration-mixing IBM from a shell-model perspective

Since the Duval-Barrett method has been used rather phenomenologically, its microscopic foundation has also been addressed. Van Isacker et al. [59] derived the strengths of the mixing interaction and the off-set energy for Cd and Hg isotopes from a simple shell-model interaction by using the OAI mapping with the generalized seniority scheme, and pointed out that, generally, while the derived off-set energy was consistent with the one obtained from a phenomenological fit to data, the derived

mixing strengths were larger than the phenomenological ones. In Refs. [3, 4] a semi-empirical expression for the energy of the intruder 0^+ state was proposed, composed of the unperturbed separation of the regular and intruder configurations (off-set energy), of the monopole correction to the proton single-particle energy, and of the energy gained by the pairing and the proton-neutron quadrupole correlations.

2.3. Group-theoretical aspects of shape coexistence

As the IBM is closely linked to group theory, a symmetry-dictated analysis of shape coexistence is also possible. The concept of intruder analog states, labelled by the I-spin quantum number, was introduced by Heyde and collaborators [22, 23] as a new class of classification scheme relevant to particle-hole excitations. A particle-like boson is represented by a spin $I = 1/2$ and its projection $I_z = +1/2$ and a hole-like boson by a spin $I = 1/2$ and its projection $I_z = -1/2$. The algebra for I-spin is analogous to that for isospin for fermions and the one for the F-spin in the proton-neutron interacting boson model (IBM-2) [14].

The I-spin symmetry was used as a guide to constrain parameters of the boson Hamiltonian in describing the structure of Pb isotopes [17] where the Hamiltonians for the $2p-2h$ and $4p-4h$ configurations were fixed by taking the parameters from adjacent even-even $Z = 78$ (Pt) and $Z = 74$ (W) isotopes, already known to give a good description of spectroscopic data. The same idea was applied to the Po isotopes [60].

In addition to the I-spin formalism, the algebraic features of particle-hole excitation modes relevant to shape coexistence were further investigated in the context of the couplings of different dynamical symmetries: U(5)-SU(3) [60], U(5)-SO(6) [61], and SO(6)-SU(3) [62].

2.4. Geometry and phases in the IBM with configuration mixing

A deformation energy surface analogous to the one in the collective model can be defined in the IBM, allowing one to *visualize* the corresponding geometry and phase transitions [63, 64]. A boson coherent state, or intrinsic state of the bosonic system $|\phi\rangle$, was introduced in Refs. [64, 65, 66], expressed, up to a normalization factor, as:

$$|\phi\rangle = \frac{1}{\sqrt{N!}}(\lambda^\dagger)^N|\mathrm{o}\rangle, \quad \text{with} \quad \lambda^\dagger = s^\dagger + \sum_\mu \alpha_\mu d^\dagger_\mu, \tag{3}$$

where proton and neutron bosons are not distinguished for simplicity, and where the five coefficients α_μ are related to the orientation of the nucleus (three Euler angles) and two intrinsic deformation variables β and γ, equivalent to those in the collective model [67]. More explicitly, $\alpha_{\pm 2} = 2^{-1/2}\beta\sin\gamma$, $\alpha_{\pm 1} = 0$ and $\alpha_0 = \beta\cos\gamma$, where $|\mathrm{o}\rangle$ represents the boson vacuum (or inert core). The expectation value of a given IBM Hamiltonian $\hat{H}_b$ in the coherent state, if written as a function of deformation parameters $|\phi(\beta,\gamma)\rangle$, provides one with the bosonic total energy surface $\langle\phi(\beta,\gamma)|\hat{H}_b|\phi(\beta,\gamma)\rangle$. Equivalent to the collective model, the bosonic energy surface generates all possible quadrupole shapes: spherical (if $\beta = 0$), prolate (if $\beta \neq 0$ and $\gamma = 0°$), oblate (if $\beta \neq 0$ and $\gamma = 60°$) and triaxial (otherwise) shapes.

Frank et al. [25] studied the geometry of the configuration-mixing IBM, with energy surfaces with more than one minimum. In Ref. [25] the intrinsic state for $np{-}nh$ ($n = 0, 2, 4, \ldots$) excitations was defined in the model space $[N]\oplus[N+2]\oplus[N+4]\oplus\cdots$.

For the system of three configurations, for instance, the expectation value of the configuration-mixing IBM Hamiltonian in Eq. (1) is expressed as the following 3×3 matrix [25]:

$$\mathcal{E}(\beta,\gamma) = \begin{pmatrix} E_0(\beta,\gamma) & \Omega_{0,2}(\beta,\gamma) & 0 \\ \Omega_{2,0}(\beta,\gamma) & E_2(\beta,\gamma)+\Delta_2 & \Omega_{2,4}(\beta,\gamma) \\ 0 & \Omega_{4,2}(\beta,\gamma) & E_4(\beta,\gamma)+\Delta_4 \end{pmatrix}, \quad (4)$$

where the diagonal and off-diagonal matrix elements stand for the expectation values of the unperturbed Hamiltonians and the mixing interactions, respectively. The three eigenvalues of $\mathcal{E}(\beta,\gamma)$ lead to specific energy surfaces, which are different from each other in topology depending mainly on the Hamiltonian parameters and off-set energies [27]. The lowest eigenvalue at each set of β and γ deformations is taken as the relevant energy surface [25]. It displays three minima, at spherical, prolate and oblate deformation, if the parameters fitted to the spectroscopic properties of the neutron-deficient Pb are taken in the Hamiltonian of Eq. (1). Along the same line, quantum phase transitions of the configuration-mixing IBM were analyzed [26], and tested in some Pt nuclei [27].

3. Mean-field derivation of the IBM

We now turn to the description of the HFB-to-IBM mapping method [31]. We start with a brief note on the mean-field calculation in Subsec. 3.1, then show how the mapping is carried out (Subsecs. 3.2, 3.3 and 3.4). We demonstrate that the method is able to describe reasonably well the low-energy spectroscopy of Sm and Ba isotopes in Subsec. 3.5, representative of axially-deformed and γ-soft nuclei, respectively.

3.1. Mean-field calculation

The first step is a standard constrained self-consistent mean-field calculation, e.g., in the Hartree-Fock-Bogoliubov (HFB) framework, based on a relativistic or non-relativistic EDF that is already shown to be valid in the global description of nuclear structure phenomena (see, e.g., reviews in Refs. [32, 38]). In this case, the constraints are on mass quadrupole moments related to the axial deformation β and non-axial deformation γ [67]. For a given set of collective coordinates (β,γ), the HFB calculations are performed to obtain an energy surface, which refers to the total mean-field energy without any symmetry projection. Neither the mass parameter nor the collective potential is considered explicitly like in some studies deriving a collective Hamiltonian from a set of EDF mean-field calculations [38, 68].

Examples of microscopic total energy surfaces are shown on the left-hand side of Fig. 2 for ^{148,150,154}Sm and ^{134}Ba nuclei. In these particular cases, the calculation was made with the constrained Hartree-Fock plus BCS (HFBCS) method [69] using the Skyrme [70, 71] EDF with the SkM* parametrization [72]. One sees in the figure that the HFBCS calculation gives a energy minimum near the origin for ^{148}Sm, a deep minimum at $\beta \approx 0.35$ for ^{154}Sm, and for ^{150}Sm a minimum soft in β direction. For ^{134}Ba, the HFBCS calculation predicts a γ-soft structure.

3.2. Mapping onto the boson space

Having the HFB total energy surface $\langle\phi_f(\beta,\gamma)|\hat{H}_f|\phi_f(\beta,\gamma)\rangle$ for each nucleus, with $|\phi_f(\beta,\gamma)\rangle$ representing the HFB solution for a given deformation (β,γ), we

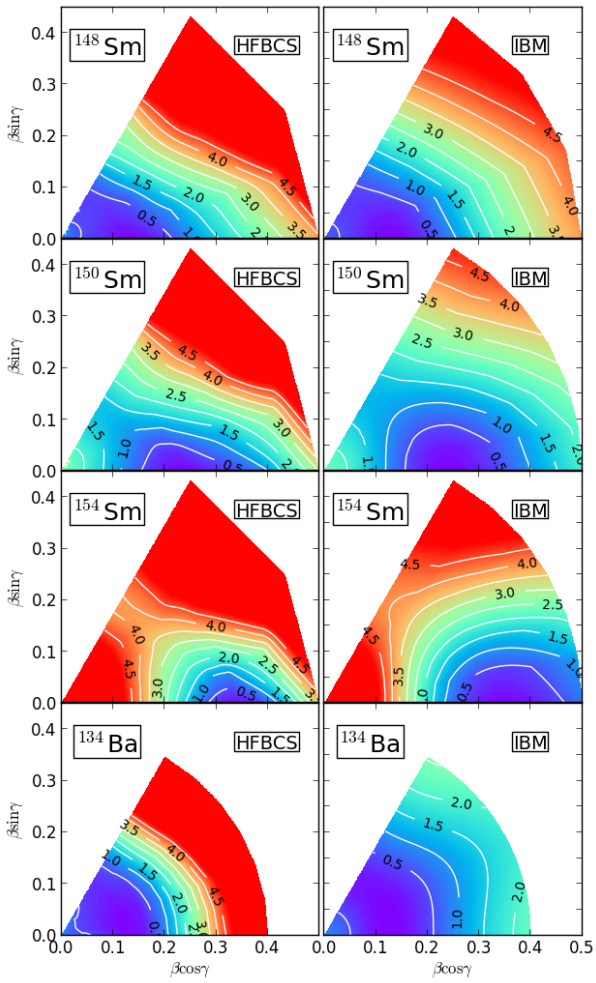

Figure 2. (Color online) Total (β, γ) energy surfaces of the ^{148,150,154}Sm and ^{134}Ba isotopes. On the left-hand side (HFBCS) are microscopic energy surfaces with the Skyrme SkM* interaction, while on the right-hand side are the mapped IBM energy surfaces. The contour lines join points with the same energy (in MeV) and the color scale varies in steps of 50 keV. The energy difference between neighboring contours is 500 keV. Data points are from Ref. [39].

subsequently map this energy surface to the corresponding energy surface of the IBM. To be more specific, the IBM Hamiltonian is constructed, i.e., the IBM strengths parameters are fixed, so as to reproduce the HFB energy surface at each set of (β, γ) as close as possible.

The coherent state (3) in the IBM-2, denoted as $|\phi_b\rangle$, is written as the product of proton λ_π and neutron λ_ν boson condensates $|\phi_b\rangle = (N_\pi! N_\nu!)^{-1/2} (\lambda_\pi)^{N_\pi} (\lambda_\nu)^{N_\nu} |\mathrm{o}\rangle$ which invokes deformation variables for both protons (β_π, γ_π) and neutrons (β_ν, γ_ν). We assume that the proton and neutron systems have the same intrinsic shapes: $\beta_\pi = \beta_\nu \equiv \beta_b$ and $\gamma_\pi = \gamma_\nu \equiv \gamma_b$. The four deformation parameters $(\beta_\pi, \beta_\nu, \gamma_\pi, \gamma_\nu)$ could in principle vary independently but, in realistic cases, introducing all of these

variables entails too much complexity. Therefore, we assume equal deformations of the proton and neutron systems, as is usual in the collective model [67]. The variable β_b in the boson system is proportional to β deformation in the collective model $\beta \propto \beta_b$ [65], while γ_b and γ have the same meaning.

Under these conditions, we equate the HFB and the IBM total energy surfaces:

$$\langle \phi_f(\beta,\gamma)|\hat{H}_f|\phi_f(\beta,\gamma)\rangle \sim \langle \phi_b(\beta_b,\gamma_b)|\hat{H}_b|\phi_b(\beta_b,\gamma_b)\rangle, \tag{5}$$

with

$$\beta = \beta_b/C_\beta, \quad \text{and} \quad \gamma = \gamma_b, \tag{6}$$

where C_β is a coefficient. Note that Eq. (5) represents an approximate equality as it is fulfilled within a limited range of (β,γ) plane, i.e., around the global minimum. We restrict ourselves to this range because it is most relevant to the low-energy collective states. One should not try to reproduce the region far from the energy minimum as the topology of the microscopic energy surface around the region is determined by single-nucleon configurations that are, by construction, outside the model space of the IBM consisting of only collective pairs of valence nucleons. For this reason, the IBM energy surface is, as shown later, always flat in the region far from the minimum. The topology of the HFB total energy surface around global minimum should reflect essential features of fermion many-body systems, such as the Pauli principle, the antisymmetrization, and the underlying inter-nucleon interactions *etc.* Through the mapping procedure, these effects are supposed to be simulated by the IBM.

The IBM Hamiltonian that embodies the essentials of the underlying fermionic interactions is taken to be of the form [11, 14]:

$$\hat{H}_b = \epsilon \hat{n}_d + \kappa \hat{Q}_\pi \cdot \hat{Q}_\nu, \tag{7}$$

where the first and second term represents, respectively, the d-boson number operator ($\hat{n}_d = \hat{n}_{d\pi} + \hat{n}_{d\nu}$), with ϵ the single d-boson energy relative to the s-boson one, and the quadrupole-quadrupole interaction with strength κ. The quadrupole operator is $\hat{Q}_\tau = d^\dagger_\tau s_\tau + s^\dagger_\tau \tilde{d}_\tau + \chi_\tau (d^\dagger_\tau \tilde{d}_\tau)^{(2)}$ ($\tau = \pi$ or ν), with χ_τ a parameter. The free parameters are ϵ, κ, χ_π, and χ_ν, plus the coefficient C_β (see Eq. (6)), and are to be fitted to the HFB total energy surface.

A technical detail in the mapping is that the IBM parameters are determined unambiguously by exploiting the technique of Wavelet Transform [73], which has been developed in the field of signal processing. More specifically, the Wavelet Transform of an IBM energy surface in the relevant range of (β,γ) is fitted to the corresponding one of an HFB energy surface by the simplex method. We note that a straightforward use of χ-square fit does not work: Due to the local topology of the microscopic energy surface that is irrelevant for low-energy collective excitations, the χ-square fit can result in many different sets of IBM parameters that do not have physical sense. The Wavelet Transform, in contrast, has the advantage of extracting the most relevant information of a given signal [73], which is, in the present case, the topology of the HFB energy surface around its minimum.

On the right-hand side of Fig. 2, we observe that the mapped IBM energy surfaces of all the nuclei considered reproduce the topology of the HFBCS counterparts in the vicinity of the absolute minima. We confirm that, compared to the original HFBCS energy surface, the one obtained from a mapped IBM looks generally flat in the region far from the minimum. As discussed before, this is a consequence of the limited model space and/or the finite boson number in the IBM framework.

3.3. Incorporating rotational response

In a strongly deformed nucleus, the rotational moment of inertia turns out to be systematically underestimated in the present method [31, 39]. This partly stems from the fact that the response of nucleonic intrinsic state to rotation is significantly different from that of the corresponding bosonic intrinsic state [40]. In order that the rotational response of fermionic and bosonic systems becomes similar, the term $\hat{L} \cdot \hat{L}$ was introduced in the IBM [40], where $\hat{L}$ stands for the angular momentum operator, and was shown to play a crucial role to improve the description of rotational spectrum in the strongly deformed nucleus [40]. Thus, for a complete description of quadrupole mode, the Hamiltonian in Eq. (7) should include this term. The $\hat{L} \cdot \hat{L}$ term affects the moment of inertia without changing other parameters already fixed through the energy-surface mapping. In Ref. [40] it was proposed to derive the $\hat{L} \cdot \hat{L}$ strength so that the cranking moment of inertia for the boson intrinsic state [74], calculated at the energy minimum, equals the cranking moment of inertia, e.g., of Thouless-Valatin [75] type, in the HFB framework at its corresponding minimum in the HFB total energy surface.

3.4. Additional degrees of freedom

Let us mention the possibility of introducing higher-order contributions in the IBM Hamiltonian. This becomes relevant especially when the energy surface has a more complex topology, e.g., γ-soft with a shallow non-axial minimum. To describe the γ-soft triaxiality in the IBM, it was shown [41] to be necessary to consider an interaction among up to three bosons, i.e., a three-boson interaction. The three-boson interaction was already introduced in a phenomenological way [76], but was considered in Ref. [41] for the first time from a microscopic perspective. An illustrative example is presented for ^{134}Ba in Fig. 2, where both the mapped IBM, which includes specific three-body boson terms, and the HFBCS energy surfaces show an almost totally γ-flat structure. One of the long-standing questions on nuclear shape has been whether a nucleus is γ unstable [77] or rather behaves as a rigid triaxial rotor [78]. On the basis of the non-relativistic and relativistic EDF calculations of the total energy surface, it was found [41] that neither of the above two geometrical pictures is realized but nuclei are somewhere in between. This finding is independent of the particular choice of the EDF, and suggests an optimal IBM description of triaxial shapes.

Another case of interest arises if the reflection symmetry of the intrinsic shape of the nucleus is broken and negative-parity states emerge. In the IBM, in addition to the positive-parity s and d bosons, it is required to include negative-parity $(p, f, \ldots)$ bosons. The octupole collective dynamics in a large number of rare-earth and light-actinide nuclei was addressed [79] based on an axially-symmetric relativistic EDF calculation of the quadrupole-octupole deformation energy surface mapped onto the *sdf* IBM [79, 80]. This represents the first EDF-based calculation of shape phase transitions, involving both quadrupole and octupole degrees of freedom.

3.5. Illustrative calculations

The diagonalization of the resultant IBM Hamiltonian, whose interaction strengths have been determined by the aforementioned ways, provides energies of and electromagnetic transition rates between excited states.

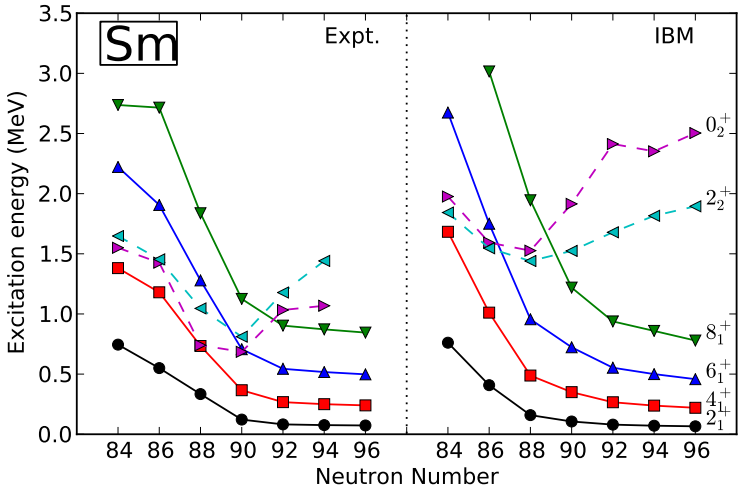

Figure 3. (Color online) Systematics of low-lying energy levels in the $^{146-158}$Sm isotopes. Calculated and experimental energies are from Refs. [39, 40] and from Ref. [81], respectively.

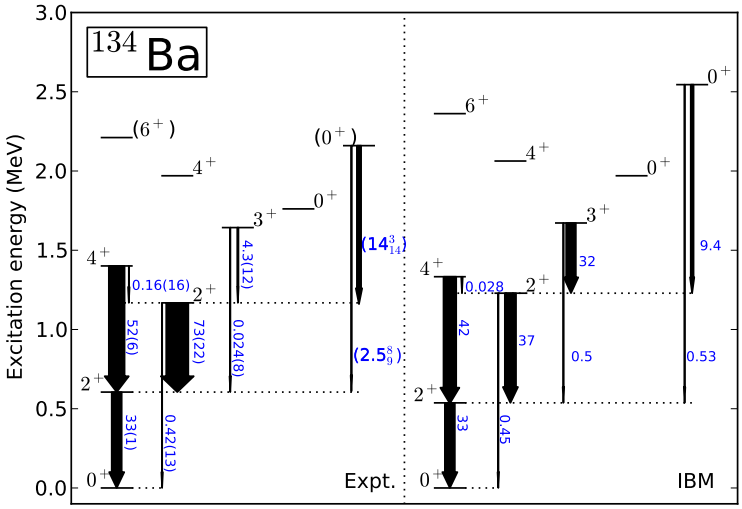

Figure 4. (Color online) Partial level scheme of ^{134}Ba, including B(E2) transition rates (in Weisskopf units). Experimental data have been taken from Refs. [81, 82]. As the experimental 0_3^+ state is uncertain [81], the corresponding B(E2) transition strengths are put in parentheses. The boson effective charges are fitted to the experimental $B(\mathrm{E2}; 2_1^+ \rightarrow 0_1^+)$ value.

We show in Fig. 3 the calculated level energies of some positive-parity yrast states of even-even $^{146-158}$Sm isotopes and the corresponding experimental data [81]. In order to follow the structural evolution with increasing mass number in a simple way, the following discussion is focused on the systematics of yrast states up to spin

8^+ and of two non-yrast 0_2^+ and 2_2^+ states. From Fig. 3, our calculation predicts that, for ^{148}Sm, the ratio $R_{4/2} = E(4_1^+)/E(2_1^+)$ is close to 2, being characteristic of vibrational nuclei, and that the yrast levels become compressed with increasing N, resulting in a typical rotational band with $R_{4/2} \approx 3.33$, especially for nuclei with $N \geq 90$. Generally, the calculation reasonably follows the experimental systematics. There is an overestimation of the non-yrast energy levels which is not consistent with the present method and needs further investigation.

We add a remark that it may not make much sense to discuss higher-spin ($J > 8^+$) and/or higher-energy (>3 MeV) states in the present framework. This is because the model space of the present IBM calculation comprising only s and d bosons may be rather limited to describe these states and because the IBM Hamiltonian is constructed only around the global minimum of a mean-field energy surface up to a few MeVs excitation energy. Furthermore, although a specific rotational cranking with non-zero angular frequency is included to fix the strength of the rotational correction term (see Subsec. 3.3), we basically refer to a static mean-field energy surface and it does not guarantee the validity of the model description of higher-spin states with typically $J > 8^+$.

We show in Fig. 4 the partial level scheme of ^{134}Ba up to around 2.0-2.5 MeV, not considering the two additional 2^+ levels at around 2 MeV [81, 82] as they are often discussed as possible mixed-symmetry states [83], being outside the scope of the present paper. In order to show that the present method is capable of describing basic features of a γ-soft nucleus, we consider levels up to around 2.0-2.5 MeV, where the IBM framework is generally valid [11, 30]. From Fig. 4, the overall spectroscopic information provided by the present calculation, including the $0_{2,3}^+$ excitation energies, the low-lying 2_2^+ excitation energy and its strong E2 transition to the 2_1^+ relative to the $B(\mathrm{E2};2_1^+ \to 0_1^+)$ value are consistent with the interpretation of a γ-soft nucleus or SO(6) limit [11] of the IBM.

At this point, we come to the conclusion that the HFB-to-IBM mapping method is able to produce energy spectra that are typical for transitional nuclei when moving away from closed shells into regions with many valence protons and neutrons – spherical vibrational, strongly deformed and γ-soft shapes – or, equivalently, three dynamical symmetries of the IBM. The derived IBM parameters have been shown [31, 39, 58] to be compatible with those used in previous phenomenological IBM calculations and those derived by the OAI mapping.

4. Extension to shape coexistence

4.1. Benchmark calculation: ^{186}Pb

In this section we demonstrate how the method can be extended to shape coexistence. Let us take the ^{186}Pb nucleus as an illustrative example. On the left-hand side of Fig. 5 is shown the (β, γ) total energy surface obtained from the constrained HFB method (see Ref. [84] for details) based on the Gogny [85] EDF with the parametrization D1M [86], where one notices three minima at spherical ($\beta \approx 0$), oblate ($\beta \approx 0.2$, $\gamma = 60°$) and prolate ($\beta \approx 0.3$, $\gamma = 0°$) configurations.

Intruder configurations in the IBM are introduced with the Duval-Barrett procedure described in Subsec. 2.1, including the fact that particle-like and hole-like bosons are not distinguished. The total Hamiltonian is given in Eq. (1), where each unperturbed Hamiltonian is specified in Eq. (7) (plus the $\hat{L} \cdot \hat{L}$ term), and the

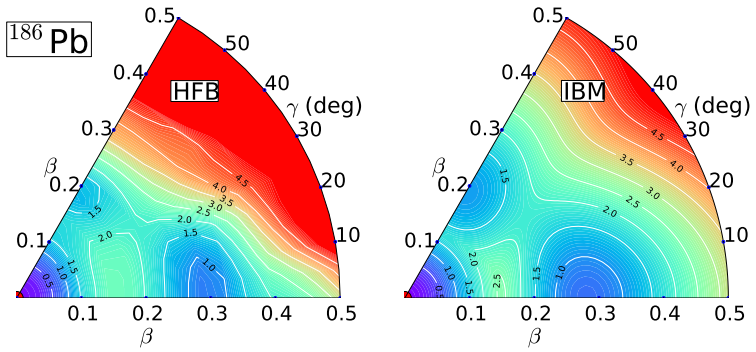

Figure 5. (Color online) Same as for the caption to Fig. 2, but for the ^{186}Pb nucleus. The results are taken from Ref. [43] and the HFB calculation is with the Gogny-D1M [86] force.

mixing interactions in Eq. (2). The bosonic energy surface is now given as the obvious extension of the formula in Eq. (4) to its IBM-2 version, under the assumption of equal proton and neutron deformation parameters.

All parameters in Eq. (1) cannot be determined simultaneously, as it would be a highly non-linear problem. Rather, they are obtained in several steps under the following assumptions.

(i) First, each unperturbed Hamiltonian $\hat{H}_n$ ($n = 0, 2, 4$) is fixed. This is done by fitting $E_n(\beta, \gamma)$ in each diagonal matrix element of $\mathcal{E}(\beta, \gamma)$ in Eq. (4) to the corresponding mean-field minimum by using the procedure described in Subsec. 3.2. Based on the empirical assignment in a mean-field picture [87], the $0p-0h$ configuration is associated with the mean-field minimum with the smallest deformation (spherical minimum of the HFB total energy surface in Fig. 5).
The same procedure is applied to the $2p-2h$ configuration to describe the minimum at oblate (or second largest) deformation and to the $4p-4h$ configuration to describe the minimum at prolate (or largest) deformation. In this way each unperturbed Hamiltonian $\hat{H}_n$ ($n = 0, 2, 4$) is determined independently, so as to reproduce the topology around the corresponding mean-field minimum.

(ii) Having determined unperturbed Hamiltonians, one then calculates the energy off-set Δ_2 (Δ_4) so that the energy difference between two neighboring minima on the HFB energy surface, corresponding to the $0p-0h$ and $2p-2h$ ($2p-2h$ and $4p-4h$) configurations, is reproduced.

(iii) Finally, the mixing terms in Eq. (2) are introduced. Their strengths $\omega_{n,n+2}$ ($n = 0, 2$) are determined so as to reproduce the overall topology of the barrier separating two neighboring mean-field minima as close as possible. We note that the inclusion of the mixing terms affects little other parameters already determined in the steps (i) and (ii): due to the inclusion of the mixing terms and the subsequent mixing, the energy difference between neighboring minima on the energy surface changes only by a few per cent in most cases. The above assumption appears to be valid as long as the values $\omega_{n,n+2} \approx 0.1 - 0.2$ MeV, which are close to those used in previous configuration-mixing IBM-2 calculations on Hg isotopes [15, 16, 50], are chosen.

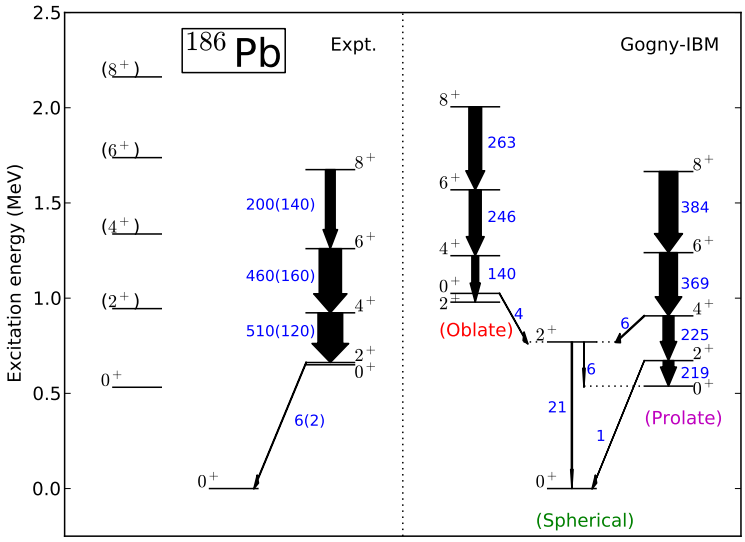

Figure 6. (Color online) Experimental and theoretical (denoted by "Gogny-IBM") partial level schemes of ^{186}Pb, including two collective bands up to spin 8^+ and the relevant B(E2) transition rates (in Weisskopf units). For clarity we mention that B(E2) values of 510(120) and 6 (2) W.u. correspond to the $4_1^+ \to 2_1^+$ and $2_1^+ \to 0_1^+$ transitions, respectively. Theoretical and experimental values are from Ref. [43] and Refs. [81, 88, 89], respectively.

The parameters of the full Hamiltonian $\hat{H}$ in Eq. (1) are determined by taking these steps, and the resultant Hamiltonian is diagonalized in the model space $[N] \oplus [N+2] \oplus [N+4]$. The corresponding mapped IBM energy surface, i.e., the lowest eigenvalue of $\mathcal{E}(\beta, \gamma)$ in Eq. (4) at each set of (β, γ), is shown on the right-hand side of Fig. 5, and exhibits three minima in accord with the HFB energy surface.

In Fig. 6 we compare the theoretical energy levels with the corresponding experimental data [81, 88, 89]. For the theoretical level scheme, the band assignment is made according to the $0p-0h$, $2p-2h$ and $4p-4h$ dominance of the wave function of each state and/or to the in-band E2 transition sequence. It is worth to note that the wave functions of low-spin states resulting from the present IBM calculation exhibit some mixing among configurations and that this is the reason why the labels "Spherical", "Oblate" and "Prolate" in Fig. 6 are put in parentheses. The boson effective charges for the E2 transition operator are taken from an earlier phenomenological IBM calculation [19]. Experimentally, two intruder bands are known up to spin 14^+ and 20^+ [89] (though with uncertainties), respectively, but as a benchmark we consider here up to spin 8^+ states, basically for the same reason as discussed in Subsec. 3.5.

From Fig. 6, our prediction that two quadrupole collective intruder bands built on low-energy 0^+ excited states appear and that the two excited 0^+ states are composed of either an oblate or prolate configuration is consistent with the experimental finding and also agrees with the results from previous beyond mean-field calculations using Skyrme [90] and Gogny [48] EDFs. The same level of quantitative agreement with experiment and with other beyond mean-field calculations [47, 48] was attained for

other neutron-deficient Pb isotopes [43].

4.2. Systematic calculation: neutron-deficient Hg isotopes

Now we turn to a more extensive application of the method to the Hg isotopes, adjacent to Pb, which exhibit also the phenomenon of shape coexistence. The calculation in this case should include up to two configurations: regular $0p-0h$ and intruder $2p-2h$, because as shown below the corresponding HFB total energy surface exhibits up to two mean-field minima.

In Fig. 7 we display the Gogny-D1M and mapped IBM (β, γ) total energy surfaces of the even-even $^{172-190}$Hg isotopes. Starting from ^{172,174}Hg, one observes a single minimum corresponding to a near-spherical configuration. The intruder prolate minimum appears in the ^{176}Hg nucleus and becomes the ground state from ^{178}Hg to ^{184}Hg corresponding to the neutron mid-shell $N = 104$ while the second lowest minimum is on the oblate side. In ^{186,188}Hg the oblate minimum becomes the ground state and, finally, in ^{190}Hg the prolate minimum disappears and only a single oblate minimum is visible. The most pronounced prolate-oblate coexistence is observed near mid-shell. Both the Gogny-D1M and mapped IBM total energy surfaces give β_2 values consistent with previous mean-field calculations within the Nilsson-Strutinsky method [87, 91] and the collective Hamiltonian approach [92] based on the Gogny D1S [93] EDF. Those studies predict $\beta_2 \approx -0.15$ and 0.25-0.3 for the oblate and prolate configurations, respectively.

Next, we show in Fig. 8 the excitation energies of the lowest two even-spin positive-parity states up to spin $J = 14^+$ in the $^{172-204}$Hg isotopes, calculated with the present method [panel (a)] and from the data [81, 94, 95, 96, 97] [panel (b)]. Experimentally, there are many low-spin states that are not uniquely identified and, for this reason, they are not shown in the plot. We first give a brief overview of the theoretical level energy systematics and then compare them with the data.

Going from ^{174}Hg to ^{176,178}Hg, the calculated 0_2^+ state rapidly drops in energy, reflecting the onset of the prolate second minimum at ^{176}Hg [see Fig. 7] and the subsequent inclusion of the intruder configuration in the IBM calculation. The significant lowering of the theoretical 0_2^+ energy level from ^{178}Hg toward the near mid-shell nuclei ^{184,186}Hg correlates with the systematics in the HFB total energy surface showing coexisting minima for these nuclei. The 0^+ ground states in $^{178-184}$Hg isotopes are predicted to be of intruder nature [see Fig. 8(a)], where the corresponding total energy surfaces predict prolate absolute minima [Fig. 7]. For heavier isotopes ($A \geq 186$), consistent with their HFB total energy surfaces, the model predicts their ground states to be of $0p-0h$ oblate nature. In Fig. 8(a) we observe that there is a jump from ^{186}Hg to ^{188}Hg in the theoretical 0_2^+ and other non-yrast states. This significant structural change is consistent with the Gogny HFB total energy surface, where we observe that the prolate minimum is less prominent in ^{188}Hg than in ^{186}Hg. From ^{190}Hg onward, for which only a single oblate configuration is required, the calculated energies of the yrast states are almost constant with mass number A, reflecting the same intrinsic structure; they increase when the $N = 126$ shell closure is approached.

Comparing our results in Fig. 8(a) with the data in Fig. 8(b), we point out the following features:

(i) First of all, the calculation describes a shape transition from the weakly deformed structures in the lightest Hg isotopes, to the manifest shape coexistence near neutron mid-shell, characterized by an approximate parabolic behavior of the

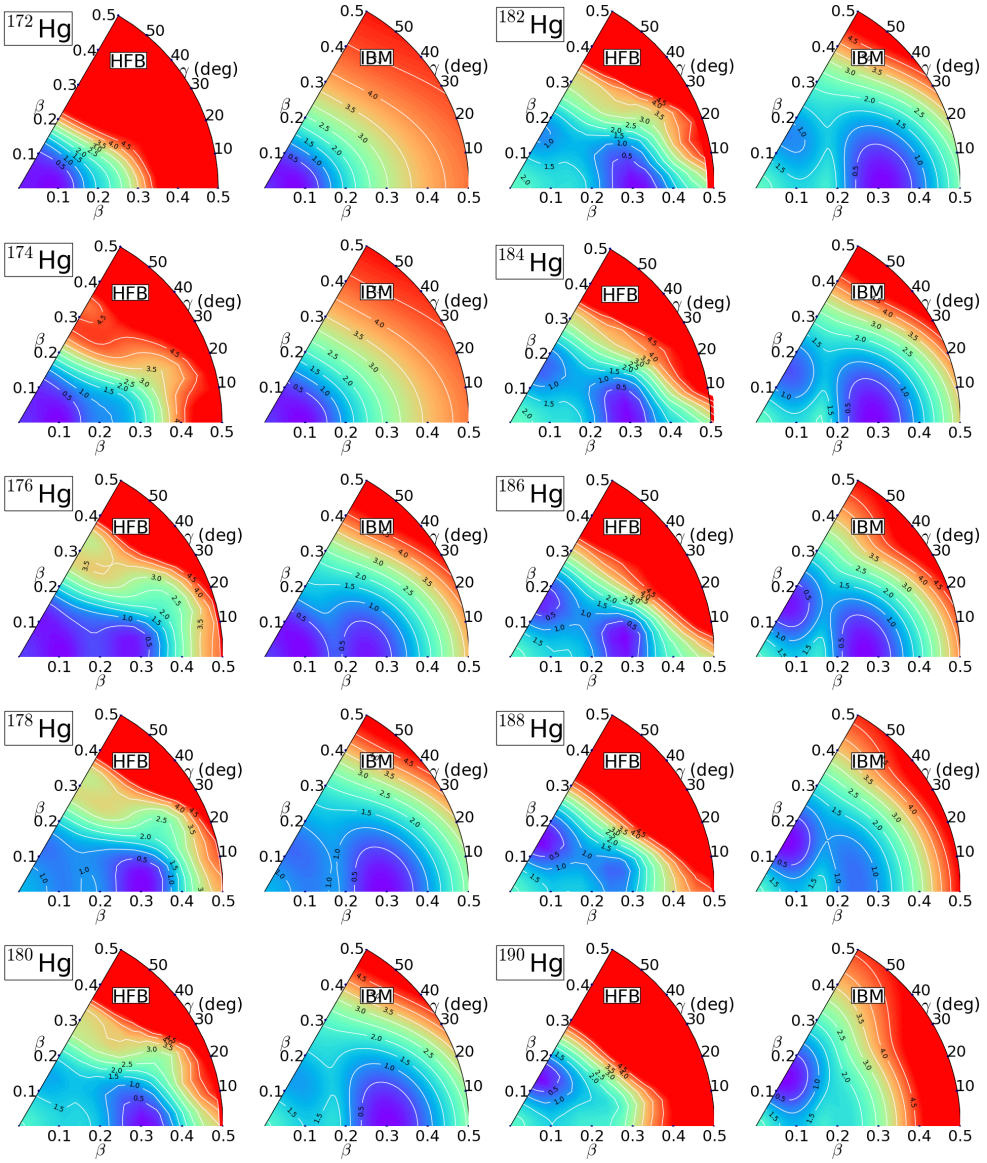

Figure 7. (Color online) Same as for the caption to Fig. 2, but for the $^{172-190}$Hg nucleus. The results are taken from Ref. [44] and the HFB calculation is with the Gogny-D1M force.

non-yrast states centered around midshell, and to the weakly oblate deformed shapes and the level structure near the $N = 126$ shell closure. Note, however, that the prediction on the states with higher spin (typically $J > 8^+$) is apparently not valid for the same reason as discussed in Subsec. 3.5.

(ii) For the near mid-shell nuclei, the wave function content (Fig. 8(a)) indicates that

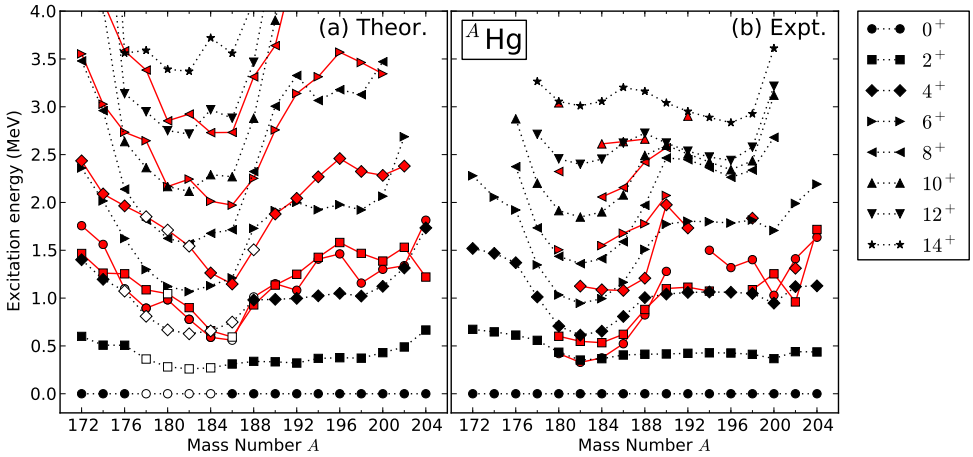

Figure 8. (Color online) Theoretical (a) and experimental (b) level energies of the lowest two even-spin positive-parity states up to 4 MeV for the even-even isotopes $^{172-204}$Hg. Dotted black and solid red lines connect the lowest and the second lowest states with a given spin, respectively. In panel (a), the 0^+, 2^+ and 4^+ states, whose wave functions are dominated by the intruder component, are represented by open symbols. Theoretical and experimental values are from Ref. [44] and Refs. [81, 94, 95, 96, 97], respectively.

the lowest two 0^+ states originate either from a regular $0p-0h$ or from an intruder $2p-2h$ configuration, consistent with the empirical knowledge.

(iii) Also for the near-midshell nuclei, particularly $^{180-184}$Hg, however, several disagreements with the experimental data are observed:

- (a) The calculation predicts the ground state 0_1^+ to be intruder prolate in nature, whereas the empirical assignment is that the oblate ground state persists all the way and that the prolate intruder state emerges when approaching the neutron midshell $N = 104$. The reason for this discrepancy is that the Gogny-D1M EDF total energy surface predicts a prolate ground state in these Hg isotopes.
- (b) The 0_2^+ energy is substantially overestimated. In the present model, the 0_2^+ excitation energy depends, to a large extent, on the prolate-oblate mean-field energy difference in the HFB energy surface. Therefore, and because of the sizable level repulsion effect due to mixing, the 0_2^+ level is pushed up in energy.
- (c) In the present calculation, some irregular patterns in band structure and B(E2) systematics for low-spin states are observed in near midshell Hg nuclei [44]. This arises from the peculiar topology of the HFB total energy surface, leading to the too strong mixing in low-spin states, and/or from the fact that the present unperturbed IBM Hamiltonians and mixing terms are too simple to describe the finer detail of the nuclei with complex shapes.

(iv) Approaching the $N = 126$ shell closure, the IBM energies of the yrast levels in $^{200-204}$Hg are stretched. The reason is that the IBM model space is too limited to describe the appearance of non-collective excitations when just a few neutron holes outside of $N = 126$ are present.

These features, revealed in this particular example of the Hg isotopes, reflect some generic aspects of the present method when it is applied to the description of complex shape dynamics. These points will be detailed in the next section.

5. Conclusions and Outlook

We have given a brief overview of studies of shape coexistence and the related spectroscopy in the framework of the IBM. To describe the phenomenon of shape coexistence, the model space including intruder excitations becomes exceedingly large in heavy open-shell nuclei, making the large-scale shell-model calculation difficult. The IBM is an approximation exploiting effective bosonic degrees of freedom and as such it is a drastic simplification of the nuclear structure calculations while preserving essential ingredients of low-energy quadrupole modes. This allows one to access heavy open-shell nuclei. Many attempts have been made in the past to incorporate intruder excitations in the IBM framework and they have been quite successful in the description of both the spectroscopic and ground-state properties which signal the shape coexistence phenomena in medium- and heavy-mass nuclei.

Here, special focus has been placed on the method developed recently by linking the self-consistent HFB approach, or equivalently the microscopic EDF framework, and the IBM. Our starting point is the HFB calculation of the total energy surface and, by mapping it onto the energy expectation value in the boson coherent state, the bosonic Hamiltonian is determined. The HFB calculation with a given EDF represents an optimal way of studying various mean-field properties all over the periodic table, and the topology of its total energy surface in the vicinity of the global minimum reflects features of many-fermion systems relevant to low-energy nuclear structure. By establishing a mapping between fermionic and bosonic total energy surfaces, those features can be simulated by the IBM system in a computationally much simpler way. The method is general so that the IBM Hamiltonian used for the spectroscopic study can be derived for any nuclear shape. This also solves the long-standing problem how to derive/understand the IBM in a comprehensive way by starting from only fermionic degrees of freedom.

The method has opened up the possibility to describe the phenomenon of shape coexistence in nuclei and its relevant spectroscopic properties. By making use of the procedure of Duval and Barrett [15], for the implementation of intruder configurations in the IBM, and of Frank et al. [25], for the coherent state for shape coexistence, the method was extended so that it describes complex shape coexistence phenomena with a microscopic input from EDF. The benchmark calculation for the neutron-deficient Pb isotopes indicates that the model description is sound in describing the two collective intruder bands built on the low-energy 0^+ excited states associated with oblate and prolate configurations. We have also shown results for neutron-deficient Hg isotopes, which are in a reasonable agreement with existing data as regards ground- and excited-state properties, including the empirical finding that the low-lying structure in the mid-shell Hg nuclei is comprised of the coexistence and mixing of oblate ground-state and prolate intruder configurations.

Nevertheless, the examples shown here also suggest the need for improvements and extensions of the model.

The first aspect concerns the assumptions that both the boson Hamiltonian used and the mapping procedure are unique, and that the Duval-Barrett procedure to explicitly incorporate the intruder excitations in the IBM is valid. Actually, as each

unperturbed Hamiltonian is not of a general form, some terms might be missing which are important to describe correctly specific low-lying states. The employed unperturbed Hamiltonians and mixing interactions might be of too simplified a form to reproduce every detail of the HFB total energy surface, which is more complicated (softer) than the bosonic energy surface, and to extract all the parameters in the unperturbed Hamiltonians, mixing strengths, off-set energies and effective charges for transition operators. To constrain better the IBM Hamiltonian, it may not be sufficient to refer to a mean-field total energy surface only, and the development of an advanced mapping might be required, invoking additional quantities, e.g., a symmetry-projected energy surface. Moreover, while we followed the assumption of Duval and Barrett that both particle and hole pairs are mapped onto the same boson, a more realistic formulation would be to consider separate mappings onto particle- and hole-like bosons and to use a single IBM Hamiltonian, instead of introducing several different Hamiltonians.

The second aspect concerns the assumption that the EDF framework gives the correct mean-field properties, including the total energy surface, which is our starting point to construct the IBM Hamiltonian. In fact, in some of the neutron-deficient Hg isotopes a prolate ground-state is predicted at the mean-field level, while it is known empirically that a weakly-oblate-deformed vibrational band stays the ground state all the way through the Hg chain and that the prolate intruder state comes lowest in energy around the mid-shell $N = 104$. This peculiar feature of the mean-field result is naturally inherited into the mapped IBM description, and it can thus happen that the intruder prolate band becomes the ground-state band in some of the Hg nuclei. However, it is worth to remark that the majority of currently available non-relativistic [49, 92, 98] and relativistic [99] EDFs, whose parameters have been determined by a global fit, commonly predict a prolate ground state at the mean-field level (and beyond) for some of the neutron-deficient Hg isotopes. The exception is the so-called NL-SC set [99] as it has been tailored to reproduce the oblate ground state in the corresponding Hg isotopes. The problem of prolate-oblate balance in the mean field is partly attributed to the single-particle spectrum, which determines the shell gap and the energy to create intruder excitations of major importance. In that sense, as investigated in Ref. [99], it would be of interest to assess the capacity of the EDF framework to predict complex shape phenomena as well as related spectroscopy.

Finally, the method to implement intruder excitations (or more than one mean-field minimum) in the IBM framework is general and could be applied to treat any deformation energy surface and the corresponding collective dynamics. This method therefore paves the way to study large-amplitude collective motions like spontaneous fission. Such a study is certainly beyond the capability of current computational power, especially as more degrees of freedom (e.g., triaxial, octupole, *etc.*) need to be included. It is nevertheless an interesting subject, and work along this line is in progress.

Acknowledgments

We would like to thank L. Guo, T. Nikšić, L. M. Robledo, R. Rodríguez-Guzmán, N. Shimizu, and D. Vretenar, for their contributions to the works reviewed in this article. K.N. acknowledges the support from the Marie Curie Actions grant within the Seventh Framework Program of the European Commission under Grant No. PIEF-GA-2012-327398.

References

[1] Morinaga H 1956 *Phys. Rev.* **101** 254
[2] Heyde K, Van Isacker P, Waroquier M, Wood J L and Meyer R A 1983 *Phys. Rep.* **102** 291
[3] Heyde K, Jolie J, Moreau J, Ryckebusch J, Waroquier M, Van Duppen P, Huyse M and Wood J L 1987 *Nucl. Phys. A* **466** 189
[4] Wood J L, Heyde K, Nazarewicz W, Huyse M and Van Duppen P 1992 *Phys. Rep.* **215** 101
[5] Andreyev A N, Huyse M, Van Duppen P *et al.* 2000 *Nature* **405** 430
[6] Heyde K and Wood J L 2011 *Rev. Mod. Phys.* **83** 1467
[7] Federman P and Pittel S 1977 *Phys. Lett. B* **69** 385
[8] Heyde K, Van Isacker P, Casten R F and Wood J L 1985 *Phys. Lett. B* **155** 303
[9] Otsuka T, Honma M, Mizusaki T, Shimizu N and Utsuno Y 2001 *Prog. Part. Nucl. Phys.* **47** 319
[10] Caurier E, Martínez-Pinedo G, Nowacki F, Poves A and Zuker A P 2005 *Rev. Mod. Phys.* **77** 427
[11] Iachello F and Arima A 1987 *The interacting boson model* (Cambridge, UK: Cambridge University Press)
[12] Arima A, Otsuka T, Iachello F and Talmi I 1977 *Phys. Lett. B* **66** 205
[13] Otsuka T, Arima A, Iachello F and Talmi I 1978 *Phys. Lett. B* **76** 139
[14] Otsuka T, Arima A and Iachello F 1978 *Nucl. Phys. A* **309** 1
[15] Duval P D and Barrett B R 1981 *Phys. Lett. B* **100** 223
[16] Duval P D and Barrett B R 1982 *Nucl. Phys. A* **376** 213
[17] Fossion R, Heyde K, Thiamova G and Van Isacker P 2003 *Phys. Rev. C* **67** 024306
[18] Fossion V H R, De Baerdemacker S and Heyde K 2005 *Phys. Rev. C* **71** 034308
[19] Hellemans V, De Baerdemacker S and Heyde K 2008 *Phys. Rev. C* **77** 064324
[20] García-Ramos J E and Heyde K 2014 *Phys. Rev. C* **89** 014306
[21] García-Ramos J E, Heyde K, Robledo L M and Rodríguez-Guzmán R 2014 *Phys. Rev. C* **89** 034313
[22] Heyde K, De Coster C, Jolie J and Wood J L 1992 *Phys. Rev. C* **46** 541
[23] Heyde K, Van Isacker P and Wood J L 1994 *Phys. Rev. C* **49** 559
[24] Coster C D, Heyde K, Decroix B, Van Isacker P, Jolie J and Lehmann H 1996 *Nucl. Phys. A* **600** 251
[25] Frank A, Van Isacker P and Vargas C E 2004 *Phys. Rev. C* **69** 034323
[26] Frank A, Van Isacker P and Iachello F 2006 *Phys. Rev. C* **73** 061302(R)
[27] Morales I O, Frank A, Vargas C E and Van Isacker P 2008 *Phys. Rev. C* **78** 024303
[28] Iachello F and Talmi I 1987 *Rev. Mod. Phys.* **59** 339
[29] Klein A and Marshalek E R 1991 *Rev. Mod. Phys.* **63** 375
[30] Mizusaki T and Otsuka T 1996 *Prog. Theor. Phys. Suppl.* **125** 97
[31] Nomura K, Shimizu N and Otsuka T 2008 *Phys. Rev. Lett.* **101** 142501
[32] Bender M, Heenen P H and Reinhard P G 2003 *Rev. Mod. Phys.* **75** 121
[33] Drut J E, Furnstahl R J and Platter L 2010 *Prog. Part. Nucl. Phys.* **64** 120
[34] Dobaczewski J 2011 *J. Phys. G: Conf. Series* **312** 092002
[35] Dobaczewski J, Bennaceur K and Raimondi F 2012 *J. Phys. G: Nucl. Part. Phys.* **39** 125103
[36] Ring P 1996 *Prog. Part. Nucl. Phys.* **37** 193
[37] Vretenar D, Afanasjev A F, Lalazissis G A and Ring P 2005 *Phys. Rep.* **409** 101
[38] Nikšić T, Vretenar D and Ring P 2011 *Prog. Part. Nucl. Phys.* **66** 519
[39] Nomura K, Shimizu N and Otsuka T 2010 *Phys. Rev. C* **81** 044307
[40] Nomura K, Otsuka T, Shimizu N and Guo L 2011 *Phys. Rev. C* **83** 041302(R)
[41] Nomura K, Shimizu N, Vretenar D, Nikšić T and Otsuka T 2012 *Phys. Rev. Lett.* **108** 132501
[42] Albers M, Warr N, Nomura K *et al.* 2012 *Phys. Rev. Lett.* **108** 062701
[43] Nomura K, Rodríguez-Guzmán R, Robledo L M and Shimizu N 2012 *Phys. Rev. C* **86** 034322
[44] Nomura K, Rodríguez-Guzmán R and Robledo L M 2013 *Phys. Rev. C* **87** 064313
[45] Albers M, Nomura K, Warr N *et al.* 2013 *Nucl. Phys. A* **899** 1
[46] Thomas T, Nomura K, Werner V, Ahn T, Cooper N, Duckwitz H, Hinton M, Ilie G, Jolie J, Petkov P and Radeck D 2013 *Phys. Rev. C* **88** 044305
[47] Bender M, Bertsch G F and Heenen P H 2006 *Phys. Rev. C* **73** 034322
[48] Rodríguez-Guzmán R, Egido J L and Robledo L M 2004 *Phys. Rev. C* **69** 054319
[49] Yao J M, Bender M and Heenen P H 2013 *Phys. Rev. C* **87** 034322
[50] Barfield A F, Barrett B R, Sage K A and Duval P D 1983 *Z. Phys. A* **311** 205
[51] Barfield A F and Barrett B R 1984 *Phys. Lett. B* **149** 277
[52] Sambataro M and Molnár G 1982 *Nucl. Phys. A* **376** 201

[53] Sambataro M 1982 *Nucl. Phys. A* **380** 365
[54] Duval P D, Goutte D and Vergnes M 1983 *Phys. Lett. B* **124** 297
[55] McCutchan E A, Casten R F and Zamfir N V 2006 *Phys. Rev. C* **71** 061301(R)
[56] García-Ramos J E and Heyde K 2009 *Nucl. Phys. A* **825** 39
[57] García-Ramos J E, Hellemans V and Heyde K 2011 *Phys. Rev. C* **84** 014331
[58] Nomura K, Otsuka T, Rodríguez-Guzmán R, Robledo L M and Sarriguren P 2011 *Phys. Rev. C* **83** 014309
[59] Van Isacker P, Pittel S, Frank A and Duval P D 1986 *Nucl. Phys. A* **451** 202
[60] De Coster C, Decroix B, Heyde K, Jolie J, Lehmann H and Wood J L 1999 *Nucl. Phys. A* **651** 31
[61] Lehmann H, Jolie J, De Coster C, Decroix B, Heyde K and Wood J L 1997 *Nucl. Phys. A* **621** 767
[62] De Coster C, Decroix B, Heyde K, Wood J L, Jolie J and Lehmann H 1997 *Nucl. Phys. A* **621** 802
[63] Gilmore R and Feng D H 1978 *Nucl. Phys. A* **301** 189
[64] Dieperink A E L, Scholten O and Iachello F 1980 *Phys. Rev. Lett.* **44** 1747
[65] Ginocchio J N and Kirson M W 1980 *Nucl. Phys. A* **350** 31
[66] Bohr A and Mottelson B R 1980 *Physica Scripta* **22** 468
[67] Bohr A and Mottelson B R 1975 *Nuclear Structure* vol 2 *Nuclear Deformations* (New York: Benjamin)
[68] Delaroche J P, Girod M, Libert J, Goutte H, Hilaire S, Péru S, Pillet N and Bertsch G F 2010 *Phys. Rev. C* **81** 014303
[69] Bonche P, Flocard H and Heenen P H 2005 *Comput. Phys. Commun.* **171** 49
[70] Skyrme T H R 1959 *Nucl. Phys.* **9** 615
[71] Vautherin D and Brink D M 1972 *Phys. Rev. C* **5** 626
[72] Bartel J, Quentin P, Brack M, Guet C and Hakansson H B 1982 *Nucl. Phys. A* **386** 79
[73] Kaiser G 2010 *A friendly guide to wavelets* (Boston: Birkhauser)
[74] Schaaser H and Brink D M 1986 *Nucl. Phys. A* **452** 1
[75] Thouless D J and Valatin J G 1962 *Nucl. Phys.* **31** 211
[76] Van Isacker P and Chen J Q 1981 *Phys. Rev. C* **24** 684
[77] Wilets L and Jean M 1956 *Phys. Rev.* **102** 788
[78] Davydov A S and Filippov G F 1958 *Nucl. Phys.* **8** 237
[79] Nomura K, Vretenar D and Lu B N 2013 *Phys. Rev. C* **88** 021303(R)
[80] Nomura K, Vretenar D, Nikšić T and Lu B N 2014 *Phys. Rev. C* **89** 024312
[81] Brookhaven National Nuclear Data Center http://www.nndc.bnl.gov
[82] Pascu S, Cătа-Danil G, Bucurescu D *et al.* 2010 *Phys. Rev. C* **81** 014304
[83] Pietralla N, von Brentano P and Lisetskiy A F 2008 *Prog. Part. Nucl. Phys.* **60** 225
[84] Rodríguez-Guzmán R, Sarriguren P, Robledo L M and García-Ramos J E 2010 *Phys. Rev. C* **81** 024310
[85] Dechargé J, Girod M and Gogny D 1975 *Phys. Lett. B* **55** 361
[86] Goriery S, Hilaire S, Girod M and Péru S 2009 *Phys. Rev. Lett.* **102** 242501
[87] Nazarewicz W 1993 *Phys. Lett. B* **305** 195
[88] Grahn T, Dewald A, Moller O *et al.* 2006 *Phys. Rev. Lett.* **97** 062501
[89] Pakarinen J, Hellemans V, Julin R *et al.* 2007 *Phys. Rev. C* **75** 014302
[90] Duguet T, Bender M, Bonche P and Heenen P H 2003 *Phys. Lett. B* **559** 201
[91] Bengtsson R, Bengtsson T, Dudek J, Leander G, Nazarewicz W and Zhang J Y 1987 *Z. Phys. A* **334** 269
[92] Delaroche J P, Girod M, Bastin G, Deloncle I, Hannachi F, Libert J, Porquet M G, Bourgeois C, Hojman D, Kilcher P, Korichi A, Le Blanc F, Perrin N, Roussière B, Sauvage J and Sergolle H 1994 *Phys. Rev. C* **50** 2332
[93] Berger J F, Girod M and Gogny D 1984 *Nucl. Phys. A* **428** 23c
[94] Sandzelius M, Ganioğlu E, Cederwall B *et al.* 2009 *Phys. Rev. C* **79** 064315
[95] Julin R, Helariutta K and Muikku M 2001 *J. Phys. G* **27**
[96] Page R D, Andreyev A N, Wiseman D R *et al.* 2011 *Phys. Rev. C* **84** 034308
[97] Elseviers J, Andreyev A N, Antalic S *et al.* 2011 *Phys. Rev. C* **84** 034307
[98] Bender M, Bonche P, Duguet T and Heenen P H 2004 *Phys. Rev. C* **69** 064303
[99] Nikšić T, Vretenar D, Ring P and Lalazissis G A 2002 *Phys. Rev. C* **65** 054320